Hydrology research, June 2016, 47 (3) 591-605
DOI: 10.2166/nh.2015.095

Acoustic Doppler Current Profiler measurements near a weir with fish pass: assessing solutions to compass errors, spatial data referencing and spatial flow heterogeneity

Thomas Kriechbaumer[1], Kim Blackburn[2], Nick Everard[3], Monica Rivas Casado[1*]

[1] Cranfield University, School of Energy, Environmental Technology and Agrifood, UK

[2] Cranfield University, School of Aerospace, Transport Systems and Manufacturing, UK

[3] Environment Agency, Evidence Directorate, UK

* Corresponding Author: Cranfield University, College Road, Cranfield, Bedfordshire, MK43 0AL, United Kingdom, T: +44 (0) 1234 750111 x2706, E: m.rivas-casado@cranfield.ac.uk

Abstract

There has been an increasing interest in the use of Acoustic Doppler Current Profilers (ADCPs) to characterise the hydraulic conditions near river engineering structures such as dams, fish passes and groins, as part of ecological and hydromorphological assessments. However, such ADCP applications can be limited by compass errors, obstructed view to navigation satellites, frequent loss of bottom tracking and spatially heterogeneous flow leading to erroneous water velocity measurements. This study addresses these limitations by (i) developing a heading sensor integration algorithm that corrects compass errors from magnetic interference, (ii) testing a Total Station based technique for spatial ADCP data referencing and (iii) evaluating a recently proposed data processing technique that reduces bias from spatial flow heterogeneity. The integration of these techniques on a radio control ADCP platform is illustrated downstream of a weir with fish pass on the River Severn, UK. The results show that each of the techniques can have a statistically significant effect on the estimated total water velocities and can strongly affect measures of vorticity. The obtained 3-dimensional flow maps are suitable to describe the magnitude and orientation of the fish pass attraction flow in relation to competing flows and to highlight areas of increased vorticity.

Keywords: attraction flow, compass, flow measurement, inertial measurement unit, radio control boat, Total Station

INTRODUCTION

Acoustic Doppler Current Profilers (ADCPs) have evolved as a useful tool to characterise the flow distribution of river reaches (e.g. Dinehart and Burau, 2005; Rennie and Church, 2010). A number of studies (Gaeuman and Jacobson, 2005; Jamieson *et al.*, 2011, 2013; Johnson *et al*., 2009) have illustrated the potential of ADCPs to quantify the flow field near river engineering structures as part of ecological and hydromorphological assessments. These studies have highlighted a range of ADCP data quality issues, including: (i) errors in the ADCP-internal compass data caused by changes in the local magnetic field (e.g. from steel reinforcements), (ii) limited line of sight to navigation satellites when using ADCPs in conjunction with Global Navigation Satellite Systems (GNSS), (iii) discontinuous water velocity measurements caused by the loss of the ADCP Bottom Tracking (BT) signal and (iv) lack of accurate 3-dimensional (3D) water velocity measurements in spatially heterogeneous flows. These limitations reduce the applicability of ADCPs to characterise the hydrodynamics near engineered flow obstacles. For example, Jamieson *et al.* (2013) found spatial ADCP data referencing based on the Global Positioning System (GPS) to be insufficiently reliable when monitoring the hydraulics induced by stream barbs on a river in a heavily wooded and deep valley. Jamieson *et al.* (2011) experienced BT loss near a wing dike and attributed this problem to high water turbidity and turbulence and Johnson *et al.* (2009) found the ADCP data collected near surface flow outlets at dams to be biased because of large spatial flow heterogeneity.

This study introduces novel techniques of ADCP data collection and assesses a recently developed method of data post-processing to address these data quality issues. The proposed methods are integrated on a radio control ADCP platform and illustrated by quantifying the 3D distribution of water velocities immediately downstream of a weir with fish pass. The installation of fish passes at engineering structures designed to regulate discharge has been a

57 wide-spread approach to restore the longitudinal connectivity of freshwater ecosystems
58 (Katopodis and Williams, 2012). Policy efforts towards restoring the ecological integrity of
59 rivers (EC, 2007, 2000) and the increasing evidence on the low efficiencies of existing fish
60 passes (Bunt *et al.*, 2012; Noonan *et al.*, 2012) have led to a strong need for more post-
61 construction assessment to gain a better understanding of the various factors determining the
62 biological effectiveness of fish passes. The hydrodynamic conditions near fish pass entrances
63 have been recognised as a key factor influencing the ability of fish to locate and enter these
64 facilities (Lindberg *et al.*, 2013; Piper *et al.*, 2012; Williams *et al.*, 2012). Yet, there is a lack
65 of methods for the spatially continuous in-field quantification of near-pass hydrodynamics. To
66 the authors' knowledge, this paper presents the first in-field solution to rapidly quantify the
67 spatially continuous distribution of water velocities near fish pass entrances using an ADCP.
68
69 ADCPs are mono-static sensors that measure water velocities and depths by transmitting and
70 receiving acoustic pulses with three to four transducers along beams spread at an angle of
71 usually 20 to 30 degrees relative to the vertical direction. The arrangement allows for the use
72 of a single acoustic signal to obtain measurements in multiple depths along the vertical water
73 column (termed 'ensemble'; Mueller and Wagner, 2009). The water velocities measured in
74 the directions parallel to each acoustic beam are processed to resolve a 3D vector describing
75 the flow in the x, y and z directions of a coordinate system aligned with the instrument
76 (Mueller and Wagner, 2009). ADCPs have an internal fluxgate compass to determine the
77 transformation angle (β) required to reference these velocities to the local ambient magnetic
78 field (magnetic north) and, after correcting for the site-specific magnetic declination, to true
79 north. When the boat velocity is determined from ADCP-external sensors (e.g. because of BT
80 loss), the effect of moderate errors in β on the velocity components referenced to north can be
81 large as it depends on the magnitude and direction of the actual water velocity (V) and the
82 ADCP boat velocity (B). For a ratio B/V of 1, an error in β of 10° can lead to a 17% error in

the measured water velocity magnitude and an error of up to 20° in the water velocity direction (computed based on Gaeuman and Jacobson, 2005). A potential practical and low-cost solution to this limitation is the correction of ADCP compass errors with an inertial measurement unit (IMU) consisting of micro-electromechanical gyroscopes and accelerometers. Some IMUs fuse the inertial sensor data to provide orientation measurements relative to the direction of gravity, which are constrained neither in motion nor to any specific environment or location (Madgwick *et al.*, 2011).

ADCP-measured water velocities have to be corrected for boat velocities, which are typically determined from BT (Gordon, 1996). Common ADCP software flags ensembles without a valid BT signal as bad, indicating that the obtained measurements are unusable. These measurements can be recovered through the integration of external positioning systems such as GPS, based on which the boat velocity is estimated. However, fish passes and other engineered river structures are frequently installed close to river banks and these areas are particularly affected by degradation in GPS accuracy (Rennie and Rainville, 2006). The problem may increase in small rivers, where the sky view can be obstructed over a large proportion of the water surface. This limitation can be addressed through the integration of ADCPs with alternative, local positioning systems such as tracking Total Stations (TS), which achieve 3D positioning precision of sub-cm level without relying on navigation satellites (Kirschner and Stempfhuber, 2008).

Repeated ADCP measurements are necessary to capture the temporally averaged flow field in rivers (Muste *et al.*, 2004). The conventional method of repeated ADCP measurements involves the averaging of multiple 3D water velocity vectors, each of which is resolved independently from the three to four along-beam velocities measured at the same time. This method assumes that the water velocities in the areas insonified by the beams are spatially

homogeneous. The diameter of a circle enclosing the four beam footprints increases at a ratio of 0.76m per 1m increase in depth (calculated based on Rennie *et al.*, 2002, for a 1200kHz WorkHorse RioGrande ADCP). Nystrom *et al.* (2002) argued that the distance between the beam footprints is comparable to the size of large-scale turbulence, so that the assumption of homogeneous flow can easily be violated in spatially complex hydraulic conditions. The data post-processing method suggested by Vermeulen *et al.* (2014) can avoid this bias by reducing the velocity sampling volume assumed to be homogeneous. The method uses a least squares procedure to estimate the 3D velocity vector that fits best to a set of along-beam velocities measured in similar locations during repeated cross-sectional measurements. However, the approach has not been tested in ADCP applications near flow obstacles.

The aim of this study was to integrate ADCPs with external sensors and novel data processing techniques for the accurate, in-field and rapid quantification of the spatially continuous 3D water velocity distribution near fish pass entrances. This was achieved through three core objectives:

(1) develop an IMU-based heading sensor integration algorithm that corrects ADCP compass data biased by magnetic interference,

(2) test a TS-based technique that provides spatially referenced ADCP data in areas of limited sky view and determines boat velocities in areas of BT loss, and

(3) evaluate the derivation of 3D water velocities as suggested in Vermeulen *et al.* (2014) to address the ADCP data bias caused by spatial flow heterogeneity.

METHODS

Case study site

The study site was a 55m reach immediately downstream of Shrewsbury Weir on the River Severn (Figure 1). The River Severn is the longest river in the United Kingdom (UK) and one

of its main salmon rivers (NASCO, 2009). It flows from Plynlimon, Ceredigion, in the Welsh mountains to Gloucestershire, where it discharges into the British Channel. A total of 41 obstructions, with nine of them being considered significant barriers to upstream fish migration, can be identified along the course of the river. Shrewsbury Weir is the last major migration barrier to Atlantic Salmon (*Salmo salar*) before spawning grounds in the upper catchments. This study focused on the fish pass installed on the right river bank, constructed in 1976 as a pool and weir pass and then refurbished in 2006 as a deep vertical slot pass. Throughout the study, the streamwise direction was defined to be orthogonal to the weir crest (Figure 1).

Data collection

Velocity and depth data were collected using a 1200 kHz WorkHorse RioGrande ADCP (Teledyne RDI, 2007) deployed from an ARC-Boat radio control platform (HR Wallingford, 2014). The data were collected along 13 cross-sectional and 8 longitudinal profiles spaced approximately four meters apart (Figure 2). Each profile was repeatedly sampled to capture the mean 3D velocity patterns. Hereafter, each cross-sectional repetition is referred to as transect. Cross sections within 28m from the weir foot as well as longitudinal profiles were sampled six times to account for larger turbulence. Cross sections further than 28m were sampled four times. The ADCP recorded velocity and depth data at an average frequency of 1.5Hz and with a mean boat speed of $0.42 ms^{-1}$. The vertical measurement resolution was set to 0.12m. The discharge was assumed to be constant and equal to $7.1 m^3 s^{-1}$ based on records from the nearest gauging station (Figure 1).

A Leica Nova MS50 (Leica Geosystems, 2015) with TS capability was used to automatically track a 360° prism installed directly above the centre of the ADCP (Figure 2). To support the accurate implementation of the sampling strategy a software application was developed in

Matlab to display the real-time boat positions against the planned cross-sectional path. This ensured that the spatial variation of the individual transects of a measurement section and the resulting loss in spatially dependent flow features (Jamieson *et al.*, 2011) were minimised. On average, 81.0% of all ensembles were at distances below 1m to a straight line fitted through the ensemble locations of the respective measurement section.

All data were recorded on a laptop mounted on the ARC-Boat and controlled on shore from another laptop via Windows Remote Desktop Connection (Figure 2). The TS data were transmitted wirelessly to the on-board laptop using a MOXA NPort W2150 wireless device server. Bespoke software was developed in C++ to record the data from the MS50 and an x-IMU inertial measurement unit (x-io Technologies, 2012). The ADCP data were recorded using the ADCP software WinRiver II by Teledyne RD Instruments Inc. To enable temporal synchronisation of the sensors, their data were time stamped with the Windows PC time of the logging computer (for TS and IMU) and the ADCP-internal real-time clock (for the ADCP). To keep the accumulated drift of the real-time clock below 0.05s, the absolute time of the clock was set by the Windows PC time of the logging computer at least every 30 minutes in WinRiver II. The error of the time synchronisation depends on the recording frequencies of the sensors, which were 1.5, 5.4 and 64Hz on average for the ADCP, TS and IMU, respectively. In total, 0.56% of all ensembles had a temporal offset to the nearest TS sample above 0.15s. These were excluded from the analysis to limit the error in spatial data referencing.

Compass correction

Temporary compass errors were corrected by integrating the absolute heading data from the ADCP-internal fluxgate compass with relative heading data from the ADCP-external IMU. The ADCP-IMU integration algorithm detects biased ADCP compass data through cross-

correlation analysis of the time synchronised compass and IMU data within a shifting window of length *w* and for lags of -1, 0 and 1 (Figure 3). The data within a window were considered biased if none of the three cross-correlation coefficients was positive and significant ($\alpha=0.05$). The window was shifted by *w/2* until the end of the data series was reached. Data detected as biased were then replaced by corrected heading values H_{CORR}, which were computed as shown in Eq. (1).

$$H_{CORR}(i) = H_{COMP}(i\text{-}d) + H_{IMU}(i) - H_{IMU}(i\text{-}d) \quad (1)$$

where H_{COMP} are the ADCP compass heading data, H_{IMU} are the IMU heading data, *i* is the ADCP ensemble index and *d* is the distance in the data series from *i* to the centre position of the closest previous window with unbiased ADCP compass data. If the beginning of the compass data series was biased, H_{CORR} was computed as follows:

$$H_{CORR}(i) = H_{COMP}(i+d) + H_{IMU}(i) - H_{IMU}(i+d) \quad (2)$$

with *d* becoming the distance from *i* to the centre position of the closest subsequent window with unbiased compass data. Figure 3 illustrates the implementation of the algorithm using data collected at a river cross section with a steel hulled narrowboat moored on one of the river banks and affecting the local magnetic field.

The error in the compass heading ε_H was defined as shown in Eq. (3).

$$\varepsilon_H = H_{COMP} - H_{CORR} \quad (3)$$

The effects of the circular nature of degrees were accounted for (e.g. if $H_{COMP}=3$ and $H_{CORR}=359$, $|\varepsilon_H|=4$).

Spatial data referencing

The ADCP data were spatially referenced using the tracking TS. The ADCP positions were transformed to global positions in the UTM coordinate system based on reference

measurements with a differentially corrected GPS (Trimble GeoExplorer 6000 GeoXH). The positioning error (ε_P) caused by the temporal offset (Δt) between ADCP and TS data was estimated as follows:

$$\varepsilon_P = \Delta t * B_{T,BT} \quad (4)$$

where $B_{T,BT}$ is the total BT-based boat velocity for ensembles with a valid BT signal. The TS positions were used to estimate the boat velocity for ensembles (i) affected by BT signal loss or (ii) with unrealistically high BT-based total boat velocity magnitudes (> 1.4 ms^{-1}). The error (ε_B) in the total TS-based boat velocity ($B_{T,\,TS}$) was estimated as shown in Eq. (5).

$$\varepsilon_B = B_{T,\,TS} - B_{T,\,BT} \quad (5)$$

To assess whether $B_{T,BT}$ was directionally biased by a non-stationary channel bed, moving bed tests were performed in three locations of the study area (Figure 2) for durations of at least 400s each.

3D water velocity estimation

3D water velocities were estimated from the along-beam velocities using the Matlab ADCPtools implementing the method by Vermeulen *et al.* (2014). The method combines the along-beam velocity samples located within the same 3D cell of a fitted mesh. For the study at hand, the longitudinal (Δl), lateral (Δn) and vertical (Δz) mesh cell dimensions were chosen to be 2.00m, 0.40m, and 0.15m, respectively (Figure 4a). The cell size selection determines the volume for which spatially homogeneous flow is assumed, which is in contrast to conventional repeated transect ADCP data processing, where the minimum size of this volume is fixed and determined by the ADCP beam spread and measurement depth (Figure 4b). The sensitivity of the 3D velocity estimates to the mesh cell size was quantified by comparing the average number of along-beam velocity samples per cell ($\bar{x}$) and the average of the total water velocity magnitudes of the mesh cells of a cross section ($\overline{V_{T,Vermeulen}}$) for 36

237 different mesh cell sizes. The effect of the number of transects taken along a cross section on
238 $\overline{V_{T,Vermeulen}}$ was quantified by calculating the mean change in $\overline{V_{T,Vermeulen}}$ caused by
239 including another transect.
240
241 Depths and water velocities in unmeasured locations of the study area were estimated through
242 ordinary kriging as suggested by Jamieson *et al.* (2013, 2011) and Rennie and Church (2010),
243 using a 0.25x0.25m^2 grid for depths and a 0.50x0.50x0.15m^3 grid for velocities. The error (ε_V)
244 in the water velocities introduced by the spatial interpolation was quantified through cross-
245 validation (Webster and Oliver, 2007) and defined as follows:
246 $$\varepsilon_{V,m} = V_{m,\,measured} - V_{m,\,predicted} \quad (6)$$
247 where $V_{m,\,measured}$ and $V_{m,\,predicted}$ are the water velocities obtained through the method by
248 Vermeulen *et al.* (2014) and predicted through kriging in the same location, and
249 $m=\{str, crs, up\}$, which are the velocity directions in the stream coordinate system. The cross-
250 validation was carried out for a sample of 1000 points randomly selected out of the 10371
251 measurements.
252
253 **Effect of data correction techniques**
254 To assess the effects of the suggested techniques, namely (i) IMU-based compass correction,
255 (ii) TS-based recovery of ensembles with BT loss and (iii) the water velocity estimation by
256 Vermeulen *et al.* (2014), the 3D distribution of water velocities in the case study reach was
257 quantified with and without the application of each of these techniques. As counterpart to the
258 3D water velocity estimation by Vermeulen *et al.* (2014), the 3D velocities were resolved
259 using the conventional repeated transect processing method as implemented in the Matlab
260 application VMT (Parsons *et al.*, 2012). For each processing variant, the total water velocity
261 magnitudes V_T and the absolute area-weighted vorticity measure $\frac{\Gamma_{ABS}}{A_{TOT}}$ (Crowder and Diplas,

2002) were computed from the 3D flow distribution obtained after kriging interpolation and compared through descriptive statistics. Wilcoxon signed-rank tests were used to test whether the differences in V_T caused by each of the techniques were statistically significant. The vorticity measure was computed as suggested by Shields and Rigby (2005):

$$\frac{\Gamma_{ABS}}{A_{TOT}} = \frac{\sum\left|\frac{\Delta V_{up}}{\Delta crs} - \frac{\Delta V_{crs}}{\Delta up}\right| * \Delta crs * \Delta up}{\sum \Delta crs * \Delta up} \quad \text{for cross sections} \quad (7)$$

$$\frac{\Gamma_{ABS}}{A_{TOT}} = \frac{\sum\left|\frac{\Delta V_{crs}}{\Delta str} - \frac{\Delta V_{str}}{\Delta crs}\right| * \Delta str * \Delta crs}{\sum \Delta str * \Delta crs} \quad \text{for horizontal planes} \quad (8)$$

where ΔV_{str}, ΔV_{crs} and ΔV_{up} are the changes in the streamwise, cross-stream and vertical water velocities in the streamwise, cross-stream and vertical directions Δstr, Δcrs and Δup. These hydrodynamic measures were chosen because they reflect the absolute water velocity magnitudes (V_T) and the strength and abundance of spatial velocity gradients ($\frac{\Gamma_{ABS}}{A_{TOT}}$), both of which are known to affect fish swimming behaviour near fish passes (e.g. Enders *et al.*, 2009; Larinier, 2002). To explore spatial variations in the effects of the techniques, the analysis was carried out for the cross sections b, d and f shown in Figure 1 and for the horizontal planes at depths of 0.35m and 1.10m.

RESULTS

Compass correction

The ADCP-IMU integration algorithm corrected 836 ensembles (4.8% of the total number of ensembles) potentially affected by compass errors. Table 1 and Figure 5 show the statistical and spatial distribution of the detected errors. The differences in V_T obtained with and without compass correction (all other processing steps held constant) were significant in statistical terms ($\alpha=0.05$), but subtle in physical terms for all cross sections and horizontal planes analysed (Table 2).

286 **Spatial data referencing**

287 The temporal offset between the ADCP and the TS data translated to an average positioning
288 error of 0.021m and the TS-based and BT-based boat velocities showed a mean difference of
289 0.047ms^{-1} (Table 1 and Figure 6). None of the three moving bed tests suggested a non-
290 stationary channel bed based on the criterion provided in Mueller and Wagner (2009) for
291 stationary moving bed tests with external boat position reference. In total, 22.3% of the
292 ensembles (3880) had invalid BT signals. Ensembles collected in very shallow areas near the
293 edges of the study area as well as those located closer to the weir were more prone to loss of
294 BT (Figure 7). The TS-based recovery of ensembles with BT loss led to statistically
295 significant (α=*0.05*) changes in V_T only for three of the five studied sections (Table 2). For
296 cross section d, the uncorrected loss of BT led to an increase in the area-weighted vorticity by
297 more than 30%.

298

299 **3D water velocity estimation**

300 Figure 8 shows the results of the sensitivity analyses for the water velocity estimation method
301 by Vermeulen *et al.* (2014). The total number of cells for which 3D velocities could be
302 estimated and the average number of along-beam velocity samples per cell were highly
303 sensitive to changes in the mesh cell size dimensions (Figure 8a and 8b). $\overline{V_{T,Vermeulen}}$
304 showed little sensitivity to the lateral and vertical cell dimensions, but strongly decreased with
305 an increase in the longitudinal dimension up to around 1.5m (Figure 8c). The change in
306 $\overline{V_{T,Vermeulen}}$ caused by including more transects approached zero as the total number of
307 transects increased (Figure 8d). For the tested section (section b in Figure 1) the effect of
308 including the 6th and 7th transect were below 0.03ms^{-1}, respectively. Similar sensitivities were
309 found for the other measurement sections.

310

311 The results of the cross-validation for the spatial water velocity interpolation are shown in
312 Table 1 and Figure 9. The use of the 3D velocity estimation by Vermeulen *et al.* (2014)
313 instead of the conventional repeated transect processing method led to statistically significant
314 ($\alpha=0.05$) changes in V_T for three of the five sections analysed (Table 2). Moreover, using the
315 method by Vermeulen *et al.* (2014) highlighted a decrease in the area-weighted absolute
316 vorticity from cross sections b to d by 15%, whereas the conventional procedure resulted in
317 the same vorticity estimates for both cross sections.
318
319 **DISCUSSION**
320 **Performance of heading sensor integration**
321 At the case study site, only few ensembles were affected by compass errors. The largest errors
322 (up to 35°) occurred close to the left river bank and near the right bank immediately
323 downstream of the fish pass (Figure 5). It is not straightforward to attribute the detected
324 compass errors to distinct error sources. The presence of steel sheet pilings along the entire
325 left bank suggests that the errors there were caused by magnetic interference. Compass errors
326 detected further away from the banks were considerably smaller in magnitude and errors >3°
327 typically persisted over only a few ensembles. These errors might have been caused by
328 instrument dynamics as observed by Gaeuman and Jacobson (2005), who reported compass
329 errors up to 9° caused by manually rattling the ADCP mount. To the authors' knowledge, this
330 is the first study that quantifies the magnitude of ADCP compass errors in the field. Further
331 use of the suggested ADCP-IMU integration will provide additional evidence on the
332 significance of this error in ADCP-based flow mapping applications. The only prerequisite for
333 using the suggested algorithm is that the compass errors are temporary rather than persistent
334 throughout the survey. Unless the ADCP vessel itself causes permanent magnetic interference
335 (e.g. steel hulled vessels), this assumption will hold for many sites, where significant
336 magnetic interference is likely to occur only in the immediate vicinity of modified river banks

or engineering structures. The sensor integration approach can be superior to the replacement of all ADCP compass data with those of another absolute heading source such as a GPS compass (Zhao *et al.*, 2014), because (i) it does not involve problems of heading misalignment between the ADCP and the external heading source and (ii) does not depend on environmental factors such as clear sky view to GPS satellites.

Performance of Total Station based ADCP positioning

This study illustrated that tracking TS can be integrated with ADCPs using WIFI and bespoke data logging software to achieve cm-level 3D positioning accuracy independent from navigation satellites. The major limitation of tracking TS in ADCP applications is the requirement of line of sight to the tracked reflector. Permanent loss of line of sight requires the operator to regain lock to the prism. In this study, this was complicated by permanent boat motion and increased the overall time for data collection. Given the high precision of tracking TS and the relatively low measurement distances to the prism (maximum of 95.37m), it can be assumed that errors in time synchronisation contributed by far the most to the total error in spatial ADCP data referencing. ADCPs commonly used in river research are limited in their capabilities of low-latency external triggering, so that the integration of the TS relies on temporal alignment of ADCP and TS data during post-processing, which is not an optimal solution. Time synchronisation errors may also largely explain the discrepancy between TS and BT in measuring boat velocities. The mean difference was larger than the $0.031 ms^{-1}$ reported by Rennie and Rainville (2006) for Real Time Kinematic (RTK) GPS with 10Hz recording frequency.

Performance of 3D velocity estimation by Vermeulen *et al.* (2014)

The method by Vermeulen *et al.* (2014) allows the user to determine the spatial resolution of the estimated 3D velocities by setting the mesh cell dimensions. In the complex flow

363 conditions near flow obstacles and in the context of fish ecology, small cell sizes are desirable
364 because: (i) they increase the reliability of ADCP measurements by decreasing the volume for
365 which spatially homogeneous flow is assumed and (ii) they provide velocities at resolutions
366 closer to ecologically meaningful spatial scales (Shields and Rigby, 2005). The sensitivity
367 analysis in this study showed that the estimated velocity magnitudes can be highly sensitive to
368 the selected mesh cell dimensions, so that a further decrease in the cell size relies on a
369 sufficiently large number of along-beam velocity samples per cell. This might be achieved by
370 further decreasing the boat track variability, which, in this study, could have potentially led to
371 an increase in the number of along-beam samples per mesh cell of approximately one third
372 (Figure 8b). However, the distinct surface flow patterns near the weir made it difficult to
373 follow straight transect lines with the radio control boat, but relatively easy to follow previous
374 (curved) boat tracks. The current implementation of the 3D velocity derivation by Vermeulen
375 *et al.* (2014) supports the estimation of a straight mesh. Future research should look into the
376 estimation of a non-linear mesh to enable a further increase in the spatial resolution of the
377 estimated 3D velocities and raise the usefulness of ADCPs in fish-ecological studies.
378
379 A larger number of along-beam velocity samples per cell could also be achieved by increasing
380 the number of repeated transects per section or the measurement duration per transect. There
381 is little guidance to a priori determine the number of repeated ADCP transects required to
382 capture the cross-sectional distribution of temporally averaged water velocities. Petrie *et al.*
383 (2013) found four transects to be suitable to identify general trends in the streamwise velocity
384 component but insufficient to describe the temporally averaged cross-stream velocities in
385 bends of the lower Roanoke River (United States). However, the findings by Vermeulen *et al.*
386 (2014) indicate that their data processing approach requires considerably less repeated
387 transects to obtain a robust estimate of the mean velocity vector than the conventional
388 processing approach. Although this finding remains yet to be confirmed by comparison to

389 reference measurements, e.g. from a fixed vessel, it would make the technique by Vermeulen
390 *et al.* (2014) particularly suitable for studies mapping the spatial flow distribution of river
391 reaches. In practice, such studies are often carried out under time constraint so that an increase
392 in the number of transects per section comes at the cost of a decrease in the spatial density of
393 the sampled sections. The latter can increase the error introduced by spatial velocity
394 interpolation, particularly in spatially complex flow conditions (e.g. Jamieson *et al.,* 2011).
395
396 In this study, the 3D velocity components in unmeasured locations were predicted by
397 applying kriging separately to the streamwise, cross-stream and vertical velocity components,
398 the direction of which was defined based on channel geometry (the weir orientation). The
399 definition of the stream coordinate system has been shown to significantly affect the
400 interpretation of velocity components, particularly the cross stream component (Lane *et al.*,
401 2000; Petrie *et al.*, 2013). While not investigated here, it may also impact the spatial
402 correlation of the respective velocity components identified in kriging and the resulting
403 interpolation.
404
405 **3D flow and bathymetry at the study site**
406 Figure 10 to 12 show the bathymetry and 3D flow downstream of Shrewsbury Weir obtained
407 using all of the ADCP data correction techniques suggested. The bathymetric map shows a
408 large scour hole (≈4m deep) near the weir foot towards the left river bank, coinciding with the
409 area of the fastest water flow from the weir (V_T up to 0.9ms^{-1}). This jet may act as a
410 competing flow that guides fish away from the pass entrance potentially leading to severe
411 delays in upstream migration, a phenomenon observed previously in tailraces of hydroelectric
412 plants (e.g. Scruton *et al.*, 2007). On the measurement day, the discharge was sufficiently low
413 for this main jet to be diverted towards the centre of the channel as it approached an area of
414 increased material accumulation and bed elevation approximately 20m downstream of the

scour hole centre. Figure 11 shows the magnitude and orientation of the fish pass attraction flow on the right river bank. Figure 12d reveals a large vortex close to the fish pass, presumably induced by the plunging flow issued from the fish pass entrance. The jet from the pass entrance developed to a more uniformly directed attraction flow further downstream (Figure 12f) where it joined the water jet from the left bank to form a 15m wide field of water velocity with similar magnitudes and directions.

Overall, the integration of the suggested ADCP data correction techniques had a statistically significant effect on the estimated velocity magnitudes and, for some cross sections, strongly affected the estimated area-weighted vorticity (Table 2). At the particular case study site in Shrewsbury, the correction of errors in the ADCP-internal compass was the only measure with a statistically significant effect on the total velocity estimates of all tested cross sections and horizontal depth planes. The TS-based recovery of ensembles affected by BT loss and the methodologies implemented to reduce bias from spatial flow heterogeneity, on the other hand, resulted in larger changes in the estimated area-weighted vorticity. Further studies are required to (i) determine the effects of the suggested technical solutions at other river sites and (ii) assess the eco-hydrological implications of the statistically significant differences they cause in near-pass hydrodynamic quantifications.

CONCLUSIONS

The integration of external sensors and sophisticated data post-processing were shown to overcome known limitations to ADCP-based 3D flow quantifications in the complex flow environments encountered near river engineering structures forming flow obstacles. The ADCP-IMU integration introduced in this paper can be useful in any ADCP application at sites potentially affected by magnetic interference and improves the current understanding of the relevance of compass errors in ADCP measurements. The suggested approach to flow

quantification near fish pass entrances can be used complementary to fish tagging and tracking studies and thereby improve the current understanding of fish passage and fish response to near-pass hydrodynamics.

ACKNOWLEDGEMENTS

The authors gratefully acknowledge the financial support of the Environment Agency, particularly Ros Wright, and the Engineering and Physical Sciences Research Council (EPSRC) through which this work was undertaken. They are also grateful to Rob Davies, Gary Bywater and Chris Bainger from the Environment Agency and Simon Stranks from Cranfield University for their support during data collection as well as Shane O'Regan from Leica Geosystems for his technical support with the MS50 MultiStation.

The authors thank two anonymous reviewers for their constructive comments that helped improving the manuscript.

455 **REFERENCES**

456 Bunt, C.M., Castro-Santos, T. & Haro, A. 2012 Performance of fish passage structures at
457 upstream barriers to migration. *River Res. Applic.* **28**, 457–478.
458
459 Crowder, D.W. & Diplas, P. 2002 Vorticity and circulation: spatial metrics for evaluating
460 flow complexity in stream habitats. *Can. J. Fish. Aquat. Sci.* **59**, 633–645.
461
462 Dinehart, R.L. & Burau, J.R. 2005 Repeated surveys by Acoustic Doppler Current Profiler for
463 flow and sediment dynamics in a tidal river. *J. Hydrol.* **314**, 1–21.
464
465 EC 2007 Council Regulation (EC) No 1100/2007 of 18 September 2007 establishing
466 measures for the recovery of the stock of European eel. *Official J. Eur. Union* L248, 17–23.
467
468 EC 2000 Directive 2000/60/EC of the European Parliament and of the Council of 23 October
469 2000 establishing a framework for community action in the field of water policy. *Official J.*
470 *Eur. Communities* L327, 1–72.
471
472 Enders, E.C., Gessel, M.H. & Williams, J.G. 2009 Development of successful fish passage
473 structures for downstream migrants requires knowledge of their behavioural response to
474 accelerating flow. *Can. J. Fish. Aquat. Sci.* **66**, 2109–2117.
475
476 Gaeuman, D. & Jacobson, R.B. 2005 *Aquatic Habitat Mapping with an Acoustic Doppler*
477 *Current Profiler: Considerations for Data Quality*. Open-File Report 2005–1163. US
478 Geological Survey, Reston, Virginia, USA.
479
480 Gordon, R.L. 1996 *Acoustic Doppler Current Profiler. Principles of Operation. A Practical*
481 *Primer.* RD Instruments. San Diego, California, USA.
482
483 HR Wallingford 2014 ARC-Boat. <http://www.hrwallingford.com/expertise/arc-boat> last
484 accessed 24 April 2015.
485
486 Jamieson, E.C., Rennie, C.D., Jacobson, R.B. & Townsend, R.D. 2011 3-D flow and scour
487 near a submerged wing dike: ADCP measurements on the Missouri River. *Water Resour. Res.*
488 **47**, 1–20.
489
490 Jamieson, E.C., Ruta, M.A., Rennie, C.D. & Townsend, R.D. 2013 Monitoring stream barb
491 performance in a semi-alluvial meandering channel: flow field dynamics and morphology.
492 *Ecohydrology* **6**, 611–626.
493
494 Johnson, G.E., Richmond, M.C., Hedgepeth, J.B., Ploskey, G.R., Anderson, M.G., Deng, Z.,
495 Khan, F., Mueller, R.P., Rakowski, C.L., Sather, N.K., Serkowski, J.A. & Steinbeck, J.R.
496 2009 *Smolt Responses to Hydrodynamic Conditions in Forebay Flow Nets of Surface Flow*
497 *Outlets, 2007*. Pacific Northwest National Laboratory, Springfield, Virginia, USA.
498
499 Katopodis, C. & Williams, J.G. 2012 The development of fish passage research in a historical
500 context. *Ecol. Eng.* **48**, 8–18.
501
502 Kirschner, H. & Stempfhuber, W. 2008 The kinematic potential of modern tracking Total
503 Stations - a state of the art report on the Leica TPS1200+. In: *Proceedings of the 1st*

International Conference on Machine Control & Guidance (H. Ingensand, W. Stempfhuber, eds.). Zurich, Switzerland, pp. 1–10.

Lane, S. N., Bradbrook, K. F., Richards, K. S., Biron, P. M. & Roy, A. G. 2000 Secondary circulation cells in river channel confluences: measurement artefacts or coherent flow structures? *Hydrol. Process.* **14**, 2047–2071.

Larinier, M. 2002 Location of fishways. *Bull. Fr. Pêche Piscic*. **364**, 39–53.

Leica Geosystems 2015 Leica Nova MS50. <http://www.leica-geosystems.com/en/Leica-Nova-MS50_103592.htm> last accessed 24 April 2015.

Lindberg, D-E., Leonardsson, K., Andersson, A.G., Lundström, T.S. & Lundqvist, H. 2013 Methods for locating the proper position of a planned fishway entrance near a hydropower tailrace. *Limnologica* **43**, 339–347.

Madgwick, S.O.H., Harrison, A.J.L. & Vaidyanathan, R. 2011 Estimation of IMU and MARG orientation using a gradient descent algorithm. In: *2011 IEEE International Conference on Rehabilitation Robotics*. Zurich, Switzerland, pp. 1–7.

Mueller, D.S. & Wagner, C.R. 2009 *Measuring Discharge with Acoustic Doppler Current Profilers from a Moving Boat*. US Geological Survey Techniques and Methods 3A-22, US Geological Survey, Reston, Virginia, USA.

Muste, M., Yu, K. & Spasojevic, M. 2004 Practical aspects of ADCP data use for quantification of mean river flow characteristics; Part I: moving-vessel measurements. *Flow Meas. Instrum.* **15**, 1–16.

NASCO 2009 *Protection, Restoration and Enhancement of Salmon Habitat Focus Area Report, EU-UK (England & Wales)*. North Atlantic Salmon Conservation Organisation, Edinburgh, UK.

Noonan, M.J., Grant, J.W.A. & Jackson, C.D. 2012 A quantitative assessment of fish passage efficiency. *Fish Fish.* **13**, 450–464.

Nystrom, E.A., Oberg, K.A. & Rehmann, C.R. 2002 Measurement of turbulence with Acoustic Doppler Current Profilers - sources of error and laboratory results. In: *Hydraulic Measurements and Experimental Methods 2002* (T.L. Wahl, C.A. Pugh, K.A. Oberg, T.B. Vermeyen, eds.). EWRI, Reston, Virginia, USA, (CD-Rom).

Parsons, D.R., Jackson, P.R., Czuba, J. A., Engel, F.L., Rhoads, B.L., Oberg, K.A., Best, J.L., Mueller, D.S., Johnson, K.K. & Riley, J.D. 2012 Velocity Mapping Toolbox (VMT): a processing and visualization suite for moving-vessel ADCP measurements. *Earth Surf. Process. Landforms* **38**, 1244–1260.

Petrie, J., Diplas, P., Gutierrez, M. & Nam, S. 2013 Combining fixed- and moving-vessel Acoustic Doppler Current Profiler measurements for improved characterization of the mean flow in a natural river. *Water Resour. Res.* **49**, 5600–5614.

Piper, A.T., Wright, R.M. & Kemp, P.S. 2012 The influence of attraction flow on upstream passage of European eel (*Anguilla anguilla*) at intertidal barriers. *Ecol. Eng.* **44**, 329–336.

555
556 Rennie, C.D. & Church, M. 2010 Mapping spatial distributions and uncertainty of water and
557 sediment flux in a large gravel bed river reach using an Acoustic Doppler Current Profiler. *J.*
558 *Geophys. Res.* **115**, 1–27.
559
560 Rennie, C.D., Millar, R.G. & Church, M.A. 2002 Measurement of bed load velocity using an
561 Acoustic Doppler Current Profiler. *J. Hydraul. Eng.* **128**, 473–483.
562
563 Rennie, C.D. & Rainville, F. 2006 Case study of precision of GPS differential correction
564 strategies: influence on ADCP velocity and discharge estimates. *J. Hydraul. Eng.* **132**, 225–
565 234.
566
567 Scruton, D.A., Booth, R.K., Pennell, C.J., Cubitt, F., McKinley, R.S. & Clarke, K.D. 2007
568 Conventional and EMG telemetry studies of upstream migration and tailrace attraction of
569 adult Atlantic salmon at a hydroelectric installation on the Exploits River, Newfoundland,
570 Canada. *Hydrobiologia* **582**, 67–79.
571
572 Shields, F.D. & Rigby, J.R. 2005 River habitat quality from river velocities measured using
573 Acoustic Doppler Current Profiler. *Environ. Manage.* **36**, 565–575.
574
575 Teledyne RDI 2007 Rio Grande ADCP. <http://www.rdinstruments.com/rio.aspx> last
576 accessed 24 April 2015.
577
578 Vermeulen, B., Sassi, M.G. & Hoitlink, A.J.F. 2014 Improved flow velocity estimates from
579 moving-boat ADCP measurements. *Water Resour. Res.* **50**, 4186–4196.
580
581 Webster, R. & Oliver, M.A. 2007 Geostatistics for Environmental Scientists. 2nd ed. Wiley,
582 Chichester, UK.
583
584 Williams, J.G., Armstrong, G., Katopodis, C., Larinier, M. and Travade, F. 2012 Thinking
585 like a fish: a key ingredient for development of effective fish passage facilities at river
586 obstructions. *River Res. Applic.* **28**, 407–417.
587
588 x-io Technologies 2012 x-IMU. < http://www.x-io.co.uk/products/x-imu/> last accessed 24
589 April 2015.
590
591 Zhao, J., Chen, Z. & Zhang, H. 2014 A robust method for determining the heading
592 misalignment angle of GPS compass in ADCP measurement. *Flow Meas. Instrum.* **35**, 1–10.
593

594

595

TABLES

Table 1. Errors in ADCP compass heading (ε_H), Total Station based positioning ($\boldsymbol{\varepsilon_P}$), boat velocity estimation ($\boldsymbol{\varepsilon_B}$) and water velocity error introduced by kriging ($\boldsymbol{\varepsilon_V}$).

		Mean	Median	Standard deviation	Sample size
Compass correction					
$\lvert\varepsilon_H\rvert$	(deg)	2.59	1.68	3.47	836
Spatial data referencing					
ε_P	(m)	0.021	0.016	0.018	13543
ε_B	(ms^{-1})	-0.001	-0.001	0.075	
$\lvert\varepsilon_B\rvert$	(ms^{-1})	0.047	0.028	0.058	
Kriging cross validation					
$\varepsilon_{V,str}$	(ms^{-1})	-0.001	-0.001	0.075	1000
$\lvert\varepsilon_{V,str}\rvert$	(ms^{-1})	0.057	0.045	0.049	
$\varepsilon_{V,crs}$	(ms^{-1})	-0.002	0.002	0.080	
$\lvert\varepsilon_{V,crs}\rvert$	(ms^{-1})	0.058	0.044	0.055	
$\varepsilon_{V,up}$	(ms^{-1})	0.000	0.000	0.022	
$\lvert\varepsilon_{V,up}\rvert$	(ms^{-1})	0.016	0.013	0.015	

Table 2. Effects of the suggested ADCP data correction techniques on the water velocity magnitude V_T and the area-weighted vorticity Γ_{ABS}/A_{TOT}; p-values < 0.05 show statistically significant effects of the respective techniques on V_T.

		V_T (ms^{-1})						$\frac{\Gamma_{ABS}}{A_{TOT}}$ (s^{-1})
Section / Plane		Min	Max	Mean	Standard deviation	Sample size	p-value	
All corrections applied								
	b	0.012	0.917	0.130	0.116	1133	-	0.061
Cross	d	0.019	0.487	0.285	0.107	526	-	0.052
	f	0.006	0.543	0.203	0.159	433	-	0.034
Horizontal	0.35	0.003	0.938	0.217	0.149	8104	-	0.066
at depth (m)	1.10	0.003	0.598	0.195	0.129	6030	-	0.073
No compass correction (all other corrections applied)								
	b	0.012	0.870	0.130	0.114	1133	0.000	0.061
Cross	d	0.020	0.488	0.287	0.107	526	0.000	0.051
	f	0.006	0.543	0.200	0.160	433	0.002	0.034
Horizontal	0.35	0.002	0.904	0.217	0.150	8104	0.000	0.066
at depth (m)	1.10	0.003	0.611	0.195	0.129	6030	0.000	0.073
No bottom tracking replacement (all other corrections applied)								
	b	0.013	0.799	0.131	0.111	1133	0.428	0.061
Cross	d	0.018	0.523	0.291	0.113	526	0.007	0.068
	f	0.004	0.499	0.198	0.156	433	0.000	0.032
Horizontal	0.35	0.002	0.881	0.211	0.144	8104	0.000	0.066
depth (m)	1.10	0.007	0.592	0.193	0.126	6030	0.243	0.073
Conventional 3D velocity estimation instead of Vermeulen *et al.* (2014; all other corrections applied)								
	b	0.003	0.607	0.119	0.093	1133	0.000	0.057
Cross	d	0.065	0.574	0.289	0.112	526	0.050	0.057
	f	0.008	0.444	0.203	0.156	433	0.808	0.027
Horizontal	0.35	0.003	0.864	0.219	0.146	8104	0.000	0.061
at depth (m)	1.10	0.003	0.825	0.200	0.135	6030	0.000	0.067
No corrections applied								
	b	0.009	0.716	0.122	0.097	1133	0.001	0.061
Cross	d	0.027	0.584	0.301	0.109	526	0.000	0.079
	f	0.010	0.466	0.204	0.159	433	0.001	0.029
Horizontal	0.35	0.003	0.868	0.219	0.148	8104	0.019	0.067
at depth (m)	1.10	0.002	0.735	0.199	0.137	6030	0.000	0.072

606 **FIGURES**

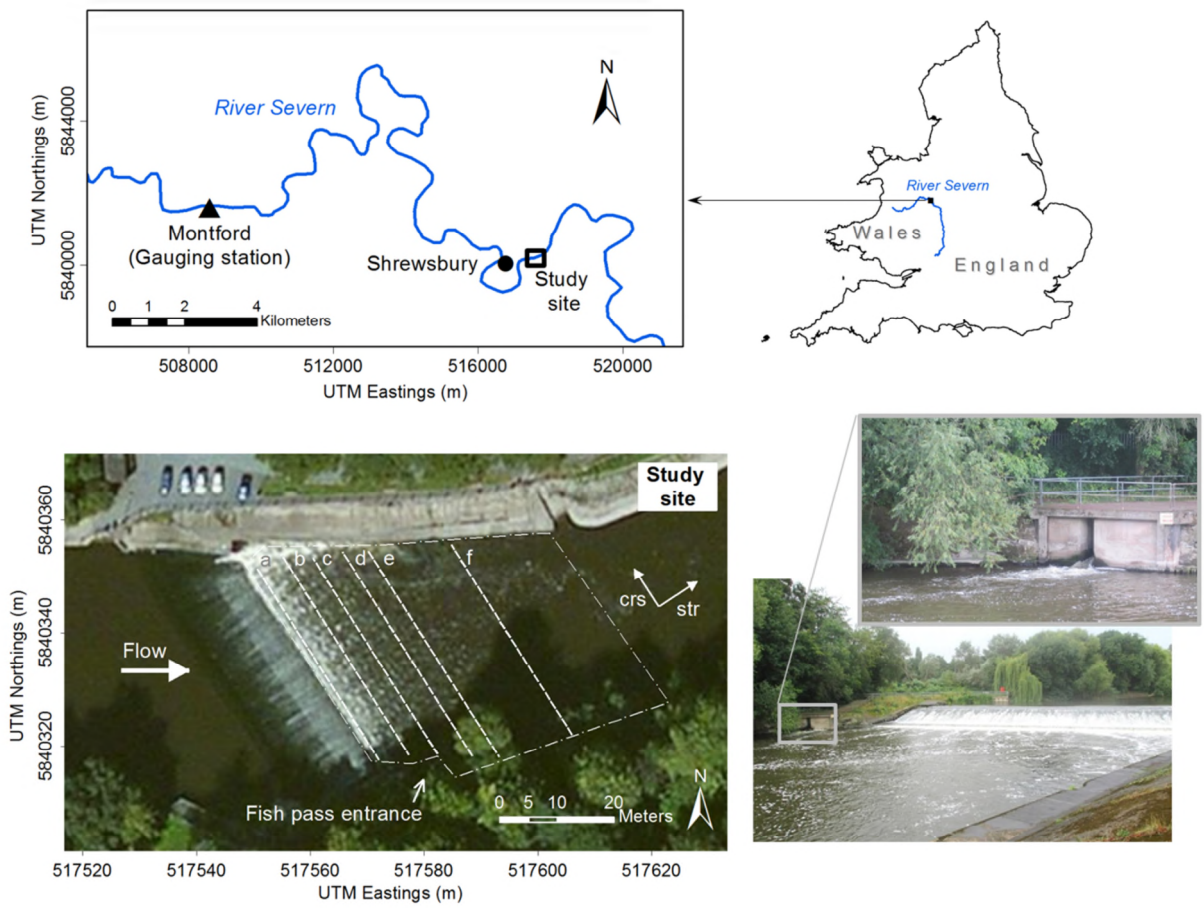

607

608 **Figure 1.** Study location; the white dash-point line depicts the extent of the study area and the white dashed lines
609 show cross sections referred to throughout the main text; the arrow pointing to the location of the fish pass
610 entrance is orientated perpendicular to the front wall of the fish pass; *str* and *crs* stand for the streamwise and
611 cross-stream directions; the images on the bottom right show the study site on the day of the data collection
612 looking in the upstream direction (20 August 2014).

613

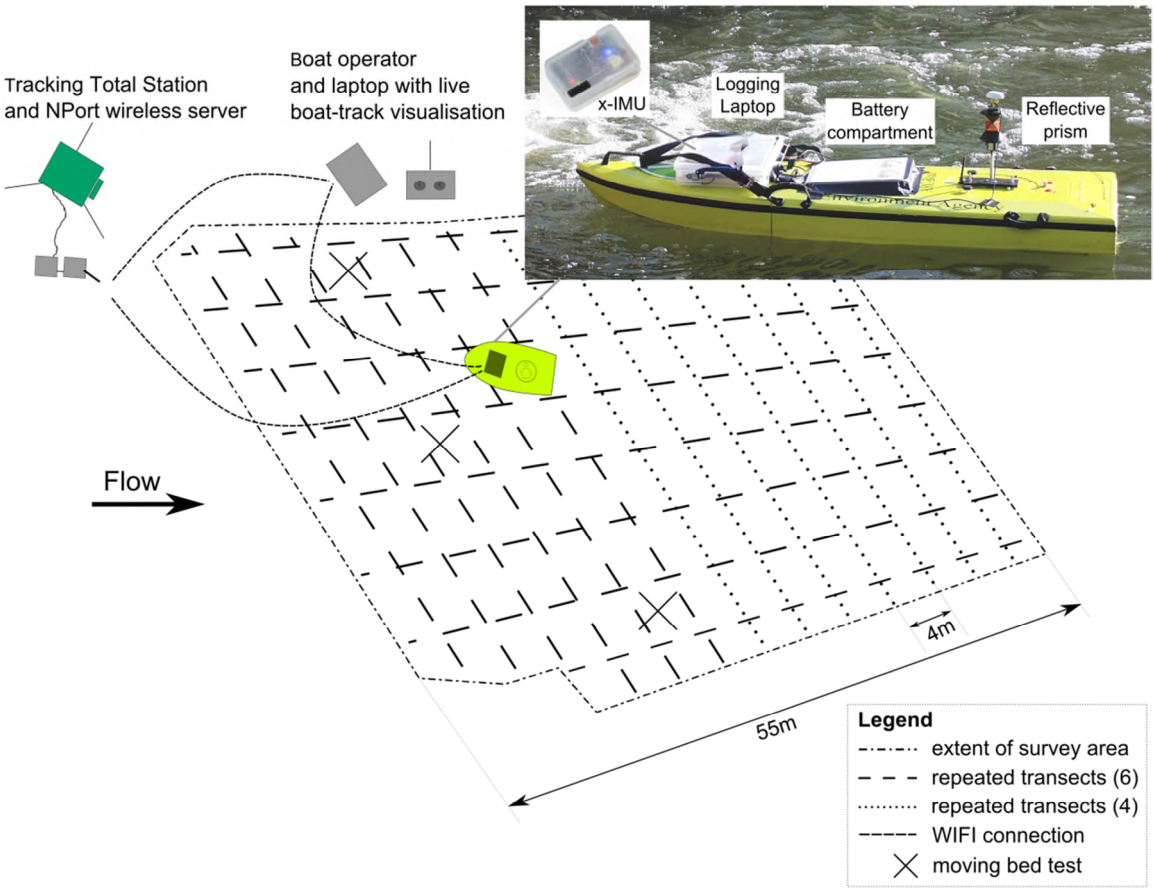

614

615 **Figure 2.** Sampling strategy and technical survey setup (not to scale).

616

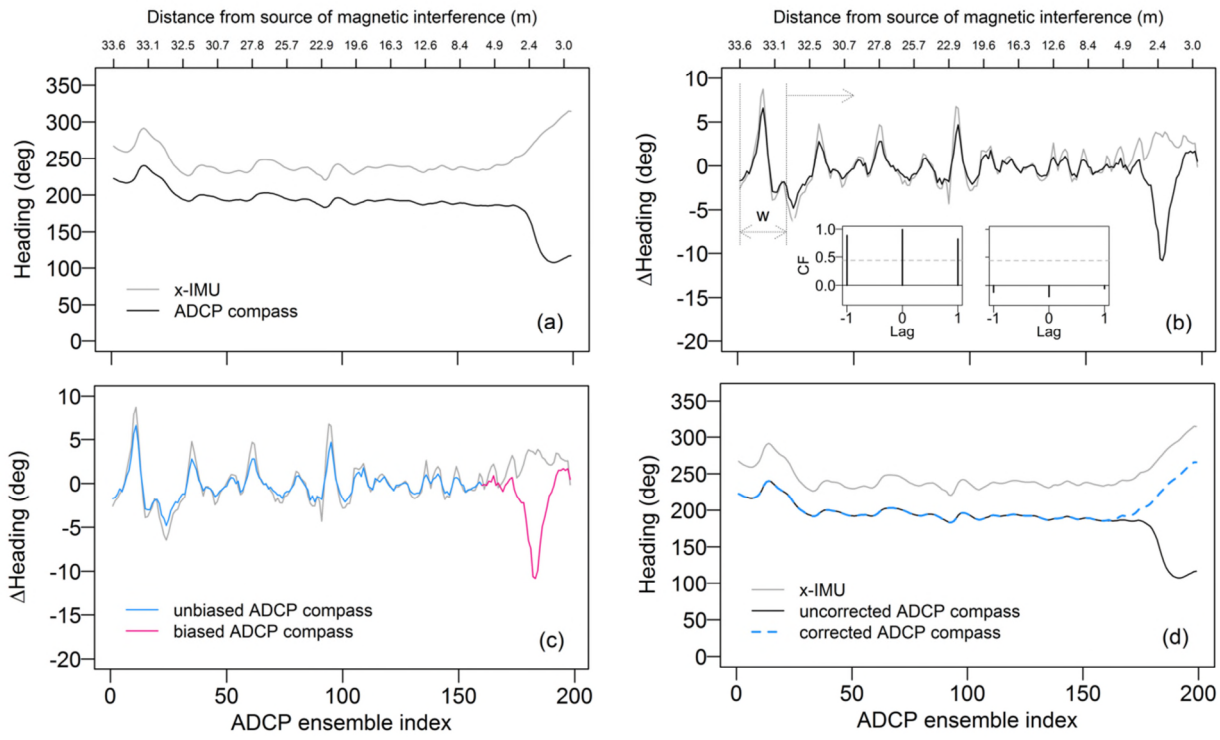

Figure 3. ADCP-IMU integration illustrated using data collected on a cross section of the River Thames at Eynsham, Oxfordshire (UK), with a moored steel hulled vessel acting as source of magnetic interference; (a) Time synchronised data of ADCP compass and x-IMU; (b) Detection of biased ADCP compass data; the two inlay plots show the results of the cross-correlation analysis for unbiased (left plot) and biased (right plot) compass data, where *CF* stands for cross-correlation function; (c) Results of the compass error detection; (d) Results of the compass error correction.

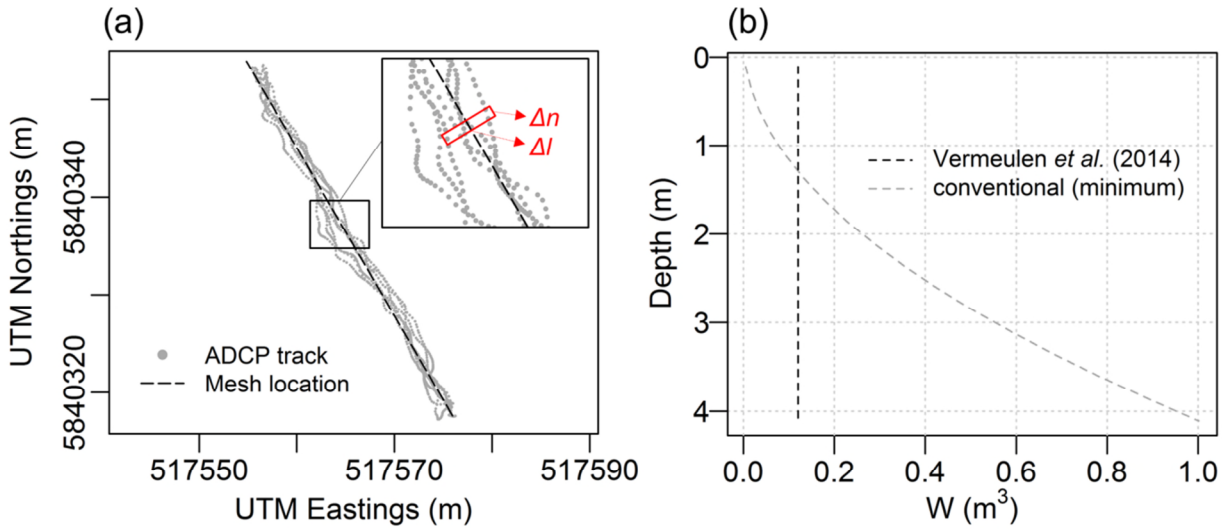

626

627 **Figure 4.** (a) Plane view of the 3D velocity projection mesh on the ADCP track (shown for section b in Figure
628 1); Δl and Δn stand for the longitudinal and the lateral mesh cell dimensions; (b) Volume ($\boldsymbol{W}$) for which spatially
629 homogeneous flow is assumed in the processing method by Vermeulen *et al.* (2014) with the cell dimensions
630 used in this study and the minimum $\boldsymbol{W}$ in conventional processing of data from a 1200 kHz WorkHorse
631 RioGrande ADCP with a vertical measurement resolution of 0.12m; an instrument draft of 0.11m was assumed
632 for both methods.

633

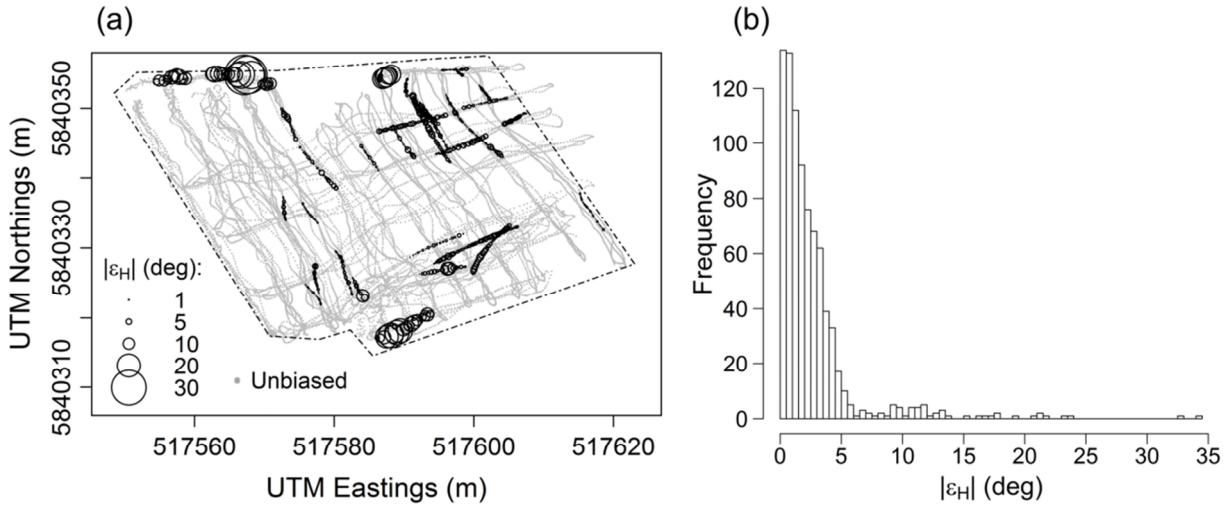

634

635 **Figure 5.** (a) Spatial distribution and magnitude of the detected absolute ADCP compass error ($|\varepsilon_H|$); the dash-

636 point line denotes the extent of the study area; (b) Statistical distribution of $|\varepsilon_H|$ (n=836).

637

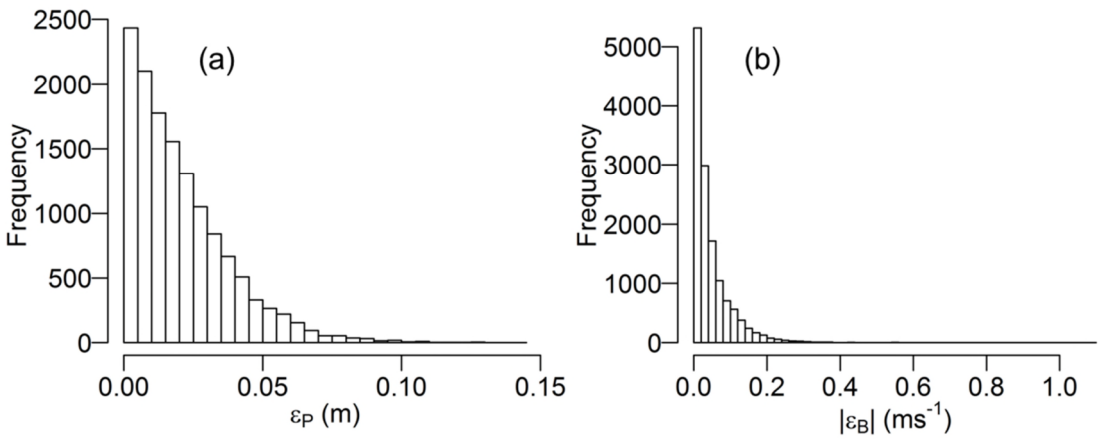

638

639 **Figure 6.** (a) Error (ε_P) in spatial data referencing caused by the temporal offset between ADCP and Total

640 Station data (n=13543); (b) Absolute error ($|\varepsilon_B|$) in the Total Station based boat velocity estimates (n=13543).

641

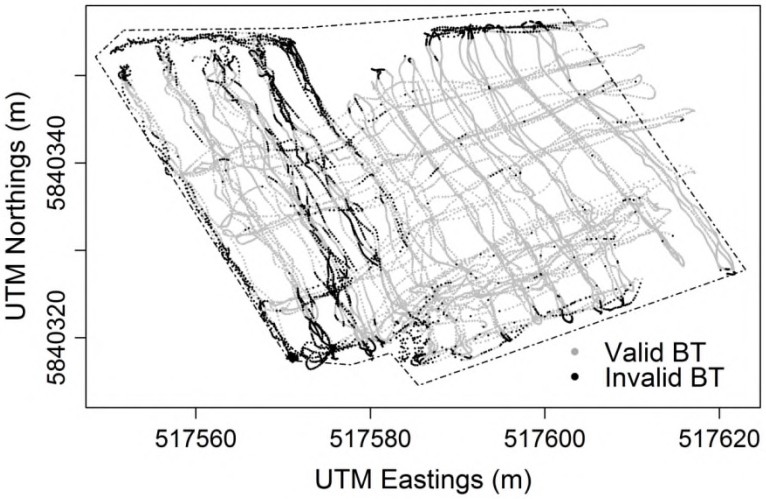

642

643 **Figure 7.** Spatial distribution of ensembles with invalid Bottom Tracking (BT) signals – the dash-point line

644 denotes the extent of the study area.

645

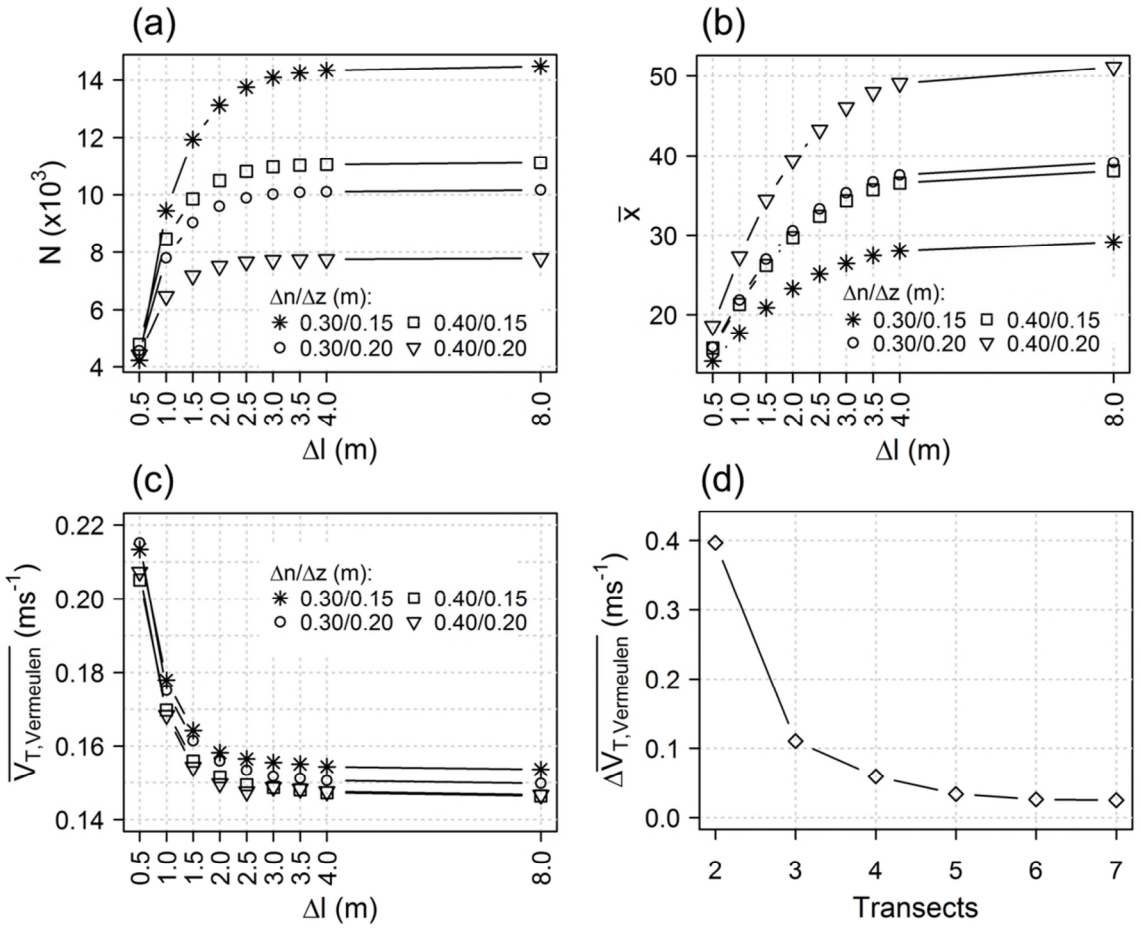

Figure 8. Sensitivity analysis for the 3D velocity estimation by Vermeulen *et al.* (2014); (a, b) Sensitivity of the total number of cells with 3D velocity estimates (N) and the average number of along-beam velocity samples per cell ($\bar{x}$) to the mesh cell dimensions (shown for the data of all sections processed); (c) Sensitivity of the estimated average water velocity magnitude in the mesh cells of a section ($\overline{\boldsymbol{V}_{\boldsymbol{T,Vermeulen}}}$) to the mesh cell dimensions (shown for the data of section b in Figure 1); (d) Change in the estimated average water velocity magnitude ($\Delta\overline{\boldsymbol{V}_{\boldsymbol{T,Vermeulen}}}$) caused by including another transect, calculated for mesh cell dimensions of Δl=2.00m, Δn=0.40m and Δz=0.15m (shown for the data of section b in Figure 1).

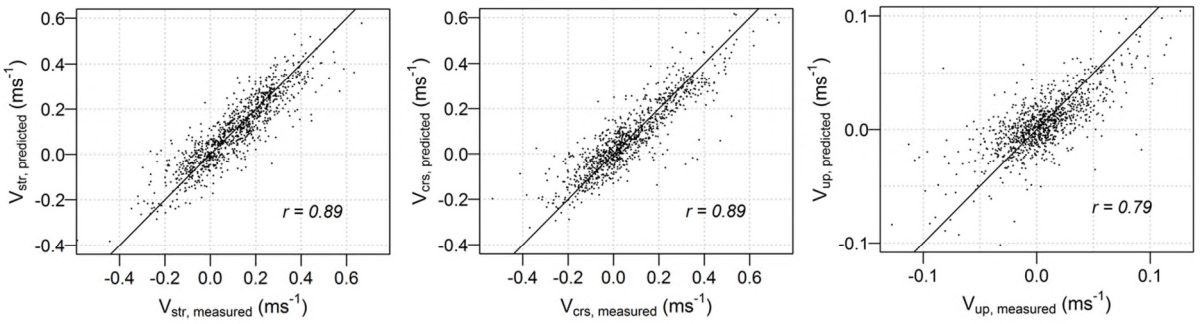

655

656 **Figure 9.** Cross-validation of spatial water velocity interpolation through ordinary kriging; *str*, *crs*, *up* and *r*
657 stand for streamwise, cross-stream and vertical and for linear correlation coefficient, respectively. The diagonal
658 line in each subplot denotes the slope of 1.

659

660

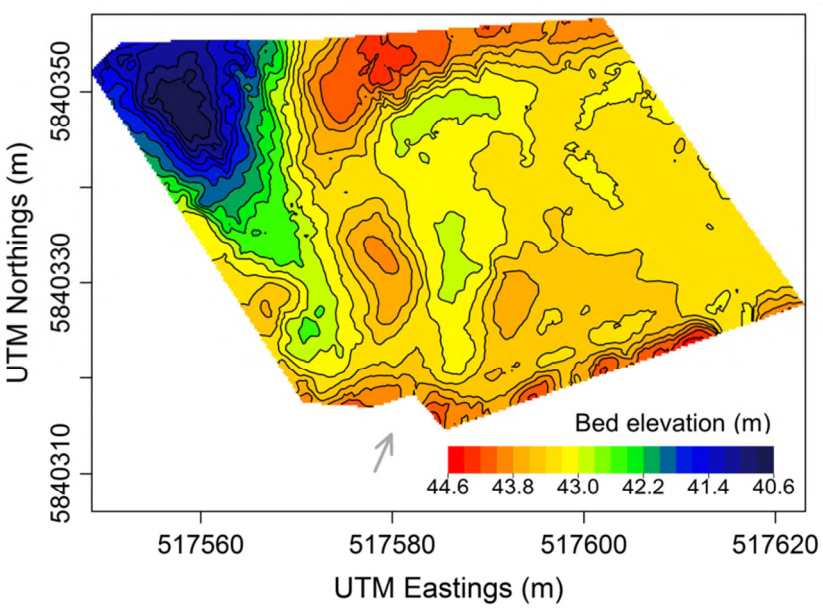

661

662 **Figure 10.** Bed elevation downstream of Shrewsbury weir; the elevation is referenced to the mean sea level as

663 obtained from GPS; the grey arrow points to the location of the fish pass entrance and is orientated perpendicular

664 to the front wall of the fish pass.

665

666

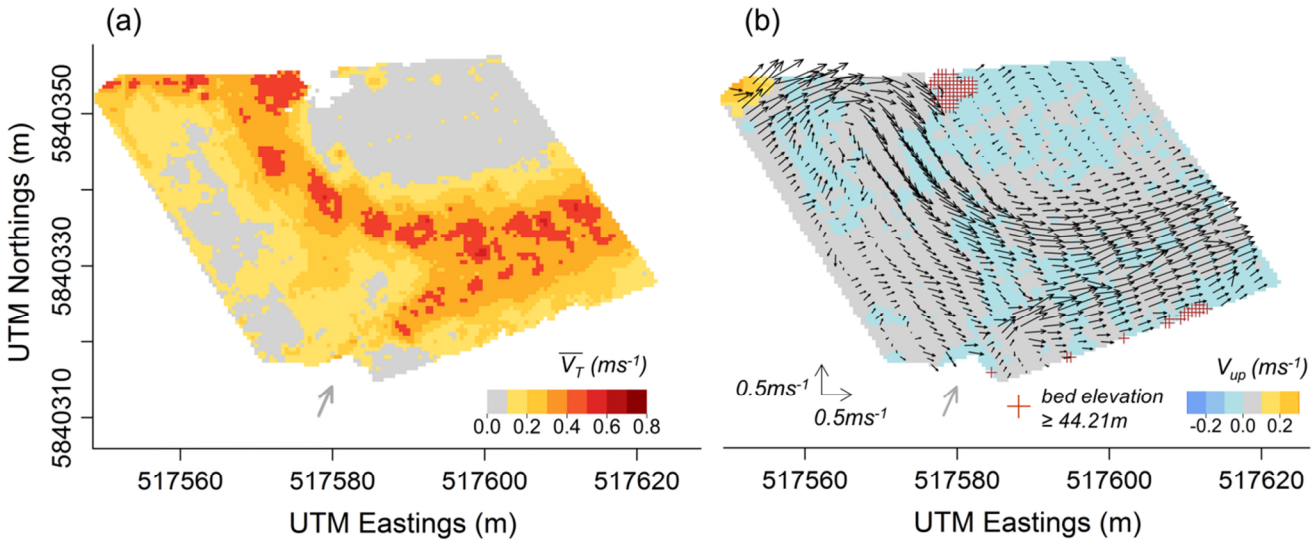

667

668 **Figure 11.** Spatial water velocity distribution downstream of Shrewsbury Weir; (a) Magnitude of depth-
669 averaged velocities ($\overline{V_T}$); (b) Streamwise and cross-stream velocities (depicted as arrows) and vertical velocities
670 (V_{up}) at an elevation of 44.21m above the sea level, corresponding to a distance of 0.35m below the mean water
671 surface elevation of the study area; the grey arrow in both plots (a) and (b) points to the location of the fish pass
672 entrance and is orientated perpendicular to the front wall of the fish pass.

673

674

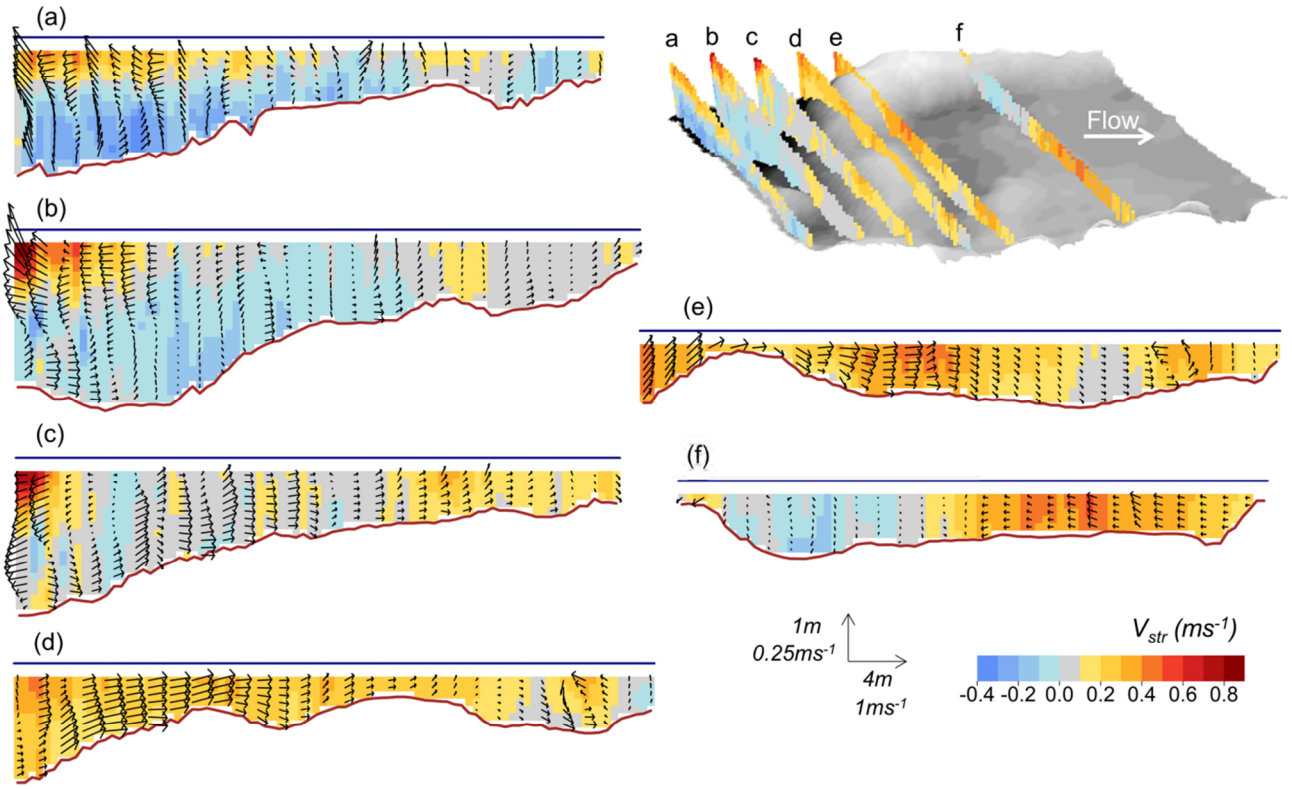

675

676 **Figure 12.** Spatial water velocity distribution at selected cross sections downstream of Shrewsbury Weir; the top
677 right plot shows the location of the cross sections on a 3D bathymetric display (see also Figure 1) and plots (a) to
678 (f) show the streamwise velocities (V_{str}) as well as the cross-stream and vertical velocities (depicted as arrows) of
679 these sections in detail.

680

681